Geosci. Model Dev. Discuss., 8, 9707–9739, 2015
www.geosci-model-dev-discuss.net/8/9707/2015/
doi:10.5194/gmdd-8-9707-2015

Geoscientific Model Development Discussions
Open Access
EGU

The location of the thermodynamic atmosphere–ice interface in fully-coupled models

A. E. West, A. J. McLaren, H. T. Hewitt, and M. J. Best

Met Office Hadley Centre, Exeter, Devon, UK

Received: 29 September 2015 – Accepted: 14 October 2015 – Published: 4 November 2015

Correspondence to: A. E. West (alex.west@metoffice.gov.uk)

Published by Copernicus Publications on behalf of the European Geosciences Union.

Abstract

In fully-coupled climate models, it is now normal to include a sea ice component with multiple layers, each having their own temperature. When coupling this component to an atmosphere model, it is more common for surface variables to be calculated in the sea ice component of the model, the equivalent of placing an interface immediately above the surface. This study uses a one-dimensional (1-D) version of the Los Alamos sea ice model (CICE) thermodynamic solver and the Met Office atmospheric surface exchange solver (JULES) to compare this method with that of allowing the surface variables to be calculated instead in the atmosphere, the equivalent of placing an interface immediately below the surface.

The model is forced with a sensible heat flux derived from a sinusoidally varying near-surface air temperature. The two coupling methods are tested first with a 1-h coupling frequency, and then a 3-h coupling frequency, both commonly-used. With an above-surface interface, the resulting surface temperature and flux cycles contain large phase and amplitude errors, as well as having a very "blocky" shape. The simulation of both quantities is greatly improved when the interface is instead placed within the top ice layer, allowing surface variables to be calculated on the shorter timescale of the atmosphere. There is also an unexpected slight improvement in the simulation of the top-layer ice temperature by the ice model. The study concludes with a discussion of the implications of these results to three-dimensional modelling. An appendix examines the stability of the alternative method of coupling under various physically realistic scenarios.

1 Introduction

Sea ice has long been recognised as an important component of the climate system, and all climate models taking part in the CMIP5 project now include a sea ice component. Much progress has been made in sea ice modelling since the 1970s. Maykut

GMDD
8, 9707–9739, 2015

and Untersteiner (1971) derived governing equations of sea ice thermodynamics, with temperature and salinity-dependent heat capacity and conductivity, and allowing for a snow layer above the ice. Semtner (1975) devised a simple numerical model of sea ice thermodynamics based on a simplification of the Maykut and Untersteiner equations, designed for incorporation in coupled climate models. An appendix to Semtner's study detailed an even simpler model in which the ice had no heat capacity at all, the so-called "zero-layer" method. The simulation of the spatial coverage of sea ice by even this highly simplified model was found to be reasonably accurate; for example, Johns et al. (2006) and Gordon et al. (2000) describe the sea ice simulations of HadGEM1 and HadCM3 respectively, both coupled models incorporating this scheme. Hence this method became the basis of the thermodynamics of many sea ice models, with its low computational costs.

As computing power increases, however, the multi-layer model of Semtner is becoming the more commonly-used version. In particular, the Los Alamos sea ice model CICE (Hunke et al., 2013), which is the focus of the present study, bases its thermodynamics on a more complex multi-layer discretisation of the Maykut and Untersteiner equations, as updated by Bitz and Lipscomb (1999), with heat capacity and conductivity fully dependent on salinity and temperature.

Currently, the configuration of models used for climate projections (HadGEM3) at the Met Office Hadley Centre uses the zero-layer version of CICE (Hewitt et al., 2011). The present study arose out of a desire to couple the multi-layer version of CICE to the Met Office atmosphere model, the Unified Model (UM) (Walters et al., 2011), and in particular its surface exchange scheme JULES (Best et al., 2011). Both CICE and JULES perform integrations using a forwards-implicit timestepping method, with much greater stability than would be associated with an explicit calculation; in CICE new ice temperatures are calculated, based on future values of temperature, conductivity, and heat capacity, while in JULES surface temperature and fluxes are calculated, based on future values of the surface exchange coefficients. CICE calculates temperatures for each of the individual ice layers, and the ice surface; JULES calculates all surface

GMDD
8, 9707–9739, 2015

variables. Hence a conflict arises when trying to couple the two components; each "wants" to calculate the surface variables itself, but in practice only one must be allowed to do so, as two different values of surface variables would be associated with two subsequently different model evolutions.

At the root of the problem is that whereas in physical reality the ice and atmospheric temperatures are intimately related, and vary in one system, in the model an explicit interface must be placed between them. Ideally one would solve implicitly for the whole ice and atmosphere column, but in practice while the two systems are separately implicit, the coupling across the interface must be explicit. CICE assumes the interface to lie above the ice surface; the JULES surface exchange scheme assumes it to lie below the ice surface. (Note that the same problem does not arise for the ice and ocean systems, because the base of the ice is at present always assumed to be at the freezing point of seawater).

The purpose of this study is to examine the two coupling methods under idealised conditions, using a one-dimensional version of the CICE temperature solver, and a miniature version of the JULES surface exchange scheme, under realistic timestep lengths, coupling period lengths, and vertical resolutions, and in particular to determine which gives the more accurate simulation. In Sect. 2, the CICE thermodynamic solver and the JULES surface energy balance solver are described in more detail, along with the two coupling methods. In Sect. 3, the performance of the CICE temperature solver is examined using its own coupling method, under varying vertical and temporal resolutions. In Sect. 4, the CICE and JULES components are run together using the two different coupling methods, and the results compared. Finally, in Sect. 5 we discuss the results, and their applicability to fully-coupled models. In the Appendix A, the stability of the alternative coupling method under the limits of physically realistic conditions is examined.

GMDD
8, 9707–9739, 2015

2 Description of the models and experiments

2.1 The models: CICE

The fundamental equation solved by the CICE temperature solver is the heat diffusion equation:

$$\rho c_p(S,T)\frac{\partial T}{\partial t} = \frac{\partial}{\partial z}\left(\kappa(S,T)\frac{\partial T}{\partial z}\right) \quad (1)$$

where ρ, c_p, S, T, t, z, and κ denote ice density, heat capacity, salinity, temperature, time, depth and conductivity respectively. CICE includes an additional term representing penetrating solar radiation, which we neglect for the purposes of this study. Conductivity and heat capacity are parametrised as

$$\kappa(S,T) = K_0 + \frac{\beta S}{T} \quad (2)$$

where

$$K_0 = 2.03\,\mathrm{W\,m^{-1}\,K^{-1}} \quad (3)$$

and

$$\beta = 0.13\,\mathrm{W\,m^{-1}} \quad (4)$$

after Untersteiner (1964) and

$$c_p = c_{p0} + \frac{L_0 \mu S}{T^2} \quad (5)$$

where

$$c_{p0} = 2106\,\mathrm{J\,kg^{-1}\,K^{-1}}, \quad (6)$$

$$L_0 = 3.354 \times 10\,\mathrm{J\,kg^{-1}} \quad (7)$$

GMDD
8, 9707–9739, 2015

and

$$\mu = 0.054\,\mathrm{K}. \tag{8}$$

after Ono (1967), respectively.

The heat diffusion equation is discretised by splitting the ice into N layers of thickness h_i, and using finite timestepping in the usual way. To ensure stability, temperatures are updated using variables from the next timestep, the so-called "implicit" method:

$$\rho_k c_{pk} \frac{T_k^{m+1} - T_k^m}{\Delta t} = \frac{1}{h_k^2}\left[K_k\left(T_{k-1}^{m+1} - T_k^{m+1}\right) - K_{k+1}\left(T_k^{m+1} - T_{k+1}^{m+1}\right)\right] \tag{9}$$

where the subscripts m and k denote timestep number and vertical layer number respectively, and $K_k = \frac{2K_{k-1}K_k}{K_{k-1}h_k + K_k h_{k-1}}$ is the "effective conductivity" at the interface between layers k and $k-1$.

There is an additional equation for the change in surface temperature, T_{sf}:

$$F_0^* + \left(\frac{\mathrm{d}F_0}{\mathrm{d}T_{\mathrm{sf}}}\right)\cdot\left(T_{\mathrm{sf}}^{m+1} - T_{\mathrm{sf}}^*\right) = K_1^*\left(T_{\mathrm{sf}}^{m+1} - T_1^{m+1}\right) \tag{10}$$

Here, F_0^* represents the sum of radiative, sensible and latent heat fluxes arriving at the ice surface from above; in the absence of melting this is equal to F_{condtop}, the conductive flux travelling downwards into the ice. Equation (10) is an approximation, as in reality upwelling longwave radiation has a nonlinear dependence on surface temperature. Starred variables represent variables from the preceding iteration.

In this way a linear system of equations for the new layer temperatures (plus the surface temperature) is created, $\mathbf{A}\boldsymbol{T}_{\mathrm{new}} = \boldsymbol{R}$, where $\mathbf{A}$ is a tridiagonal matrix and $\boldsymbol{T}_{\mathrm{new}}$ is the vector of new layer temperatures. Because the parameters c_p and K depend themselves upon the ice temperature, and because of the linear approximation in the surface equation, it is necessary to repeat the linear solver, updating outgoing longwave

GMDD
8, 9707–9739, 2015

radiation, c_p and K at each iteration, to achieve an accurate and energy-conserving solution. CICE allows up to 100 iterations, although in general fewer than 10 will suffice to reduce the energy imbalance to acceptable levels.

It should be noted that CICE also allows for the presence of a snow layer on top of the ice, which introduces an extra row into the matrix equation, with accordingly different heat capacity and conductivity. For this study, however, we assume no snow is present.

2.2 The models: JULES

The principal function of the surface-exchange scheme JULES is to solve the surface energy balance equation, in which a surface temperature is calculated such that incoming fluxes of shortwave and longwave radiation are in balance with outgoing turbulent, radiative and conductive fluxes:

$$(1-\alpha)\mathrm{SW}_{\mathrm{in}} + \mathrm{LW}_{\mathrm{in}} - \varepsilon\sigma T_{\mathrm{sfc}}^4 + F_{\mathrm{sens}}(T_{\mathrm{sfc}}, T_{\mathrm{air}}) + F_{\mathrm{lat}}(T_{\mathrm{sfc}}, T_{\mathrm{air}}, q_{\mathrm{air}}) = \kappa_{\mathrm{eff}}(T_{\mathrm{sfc}} - T_{\mathrm{ice}}) + F_{\mathrm{melt}} \quad (11)$$

In this equation $\mathrm{SW}_{\mathrm{in}}$, $\mathrm{LW}_{\mathrm{in}}$ refer to the incoming shortwave and longwave fluxes respectively; F_{sens} and F_{lat} to the net inward sensible and latent heat fluxes respectively; T_{sfc}, T_{air} and T_{ice} to surface temperature, lowest-layer air temperature and uppermost layer ice temperature respectively, q_{air} to lowest layer air specific humidity, k_{eff} to effective conductivity of the top ice layer, α to surface albedo and F_{melt} to the sea ice melt flux. JULES solves this equation by first calculating a "first guess" explicit solution, calculating fluxes and surface temperature based on surface temperature at the previous timestep, and then calculating an implicit updated solution, in which the exchange coefficients are modified by considering the initial solution. Because the surface temperature simulation carries no implications for energy conservation, the calculation is not iterated.

GMDD
8, 9707–9739, 2015

2.3 The coupling methods and experiments

In their standard formulations, both the CICE thermodynamic solver and the JULES surface exchange solver calculate surface variables. The two coupling methods under investigation arise from opposite methods of resolving this difficulty.

In the standard "CICE" coupling method (Fig. 1a), the atmosphere, or surface exchange scheme, calculates fluxes of incoming shortwave and longwave radiation based on the ice surface temperature from the previous coupling instant, averages these over the coupling period, and passes them to CICE at the end of the period. CICE then uses these incoming fluxes throughout the next coupling period in the first row of the tridiagonal matrix equation, the row concerning the surface temperature (Eq. 10), each time iterating the solver until convergence is achieved. In the process, CICE computes the remaining surface fluxes (outgoing radiative, turbulent and conductive fluxes) and hence the net surface flux. This approach is equivalent to placing an interface between JULES and CICE immediately above the ice surface.

In the alternative, "JULES" coupling method under investigation (Fig. 1b), the surface temperature is a prognostic variable of the atmosphere or surface exchange model, and is not passed from CICE; instead, the temperature and effective conductivity (the latter defined as $\frac{2K_1}{h_1}$) of the top ice layer are passed at each coupling instant. The surface exchange scheme calculates an updated surface temperature, along with radiative fluxes, turbulent fluxes, surface ice melt, and downward conductive flux into the top layer of ice from the surface, in a fully implicit boundary layer solution, given these lower boundary conditions. The downward conductive flux and ice melt flux are averaged over a coupling period and passed to CICE. CICE proceeds to solve the tridiagonal matrix occasion in the normal way, except that the top row of the equation is removed; the downwards conductive flux provided by the surface exchange scheme is then used as forcing for the top ice layer. At the end of the coupling period, the new temperature and effective conductivity of the top ice layer are passed back to the atmo-

GMDD
8, 9707–9739, 2015

sphere. This approach is equivalent to placing an interface between JULES and CICE immediately below the ice surface.

It should be noted that in HadGEM3, the two models run in parallel, with variables exchanged in each direction at every coupling instant; also, that in the "JULES" coupling method, fluxes are always passed as gridbox means, to ensure conservation.

3 Testing the impact of varying resolution on an idealised solver

3.1 Setup

In this experiment, the penetrating solar radiation term was ignored, and the ice was assumed to be fresh, in order that the conductivity and specific heat capacity are constant. The ice was assumed to be 1 m thick, and there is no snow cover. The diffusion equation was forced at the top of the ice by a sinusoidally varying heat flux:

$$F_{\mathrm{sf}} = A\mathrm{Re}(\exp i\omega t) \tag{12}$$

There exists an exact analytical solution to the diffusion equation with this surface forcing, for an infinitely deep ice cover (after Best et al., 2005):

$$T = T_{\mathrm{B}} + \frac{A}{\sqrt{\rho c \omega \kappa}} \mathrm{Re}\left(\exp\frac{-z}{l}\exp i\left(\frac{-z}{l} + \omega t - \frac{\pi}{4}\right)\right) \tag{13}$$

Where $T \to T_{\mathrm{B}}$ as $z \to \infty$. $l = \sqrt{\frac{2\kappa}{\rho c \omega}}$ is the e-folding depth.

This analytical solution was compared to the solution from the CICE temperature solver under 6 different conditions, summarised in Table 1. In these experiments, the timestep length, coupling period length and vertical resolution were varied, from extremely low values designed to give results as close as possible to "truth", to higher values considered to be typical of coupled model experiments.

GMDD
8, 9707–9739, 2015

3.2 Results

Figure 2 displays the simulation of two key variables by the temperature solver: the surface temperature, and the temperature at a depth of 0.125 m (roughly analogous to the top layer temperature in standard CICE, which uses 4 vertical layers). It is clear that under very high temporal and vertical resolution, CICE produces a simulation that is virtually indistinguishable from the analytic solution. As one would expect, when these resolutions are reduced to more realistic levels inaccuracies appear.

When the timestep length is increased to 1 h (but the high vertical resolution is maintained), there is a slight increase in the error of the surface temperature simulation, which is still very small in proportion to the cycle amplitude. For the 0.125 m temperature, a small phase lead of around 30 min is introduced, and the amplitude is reduced by a tiny amount (0.02 °C); the diurnal cycle of 0.125 m temperature error has an amplitude of about 0.03 °C.

The effect of decreasing the vertical resolution is more marked. For the surface temperature, we see a a large phase lag introduced, of 90 min, but also a marked increase in amplitude, from 1.2 to 1.5 °C; this results in some comparatively high errors, of up to 0.6 °C. On the other hand, the diurnal cycle of 0.125 m temperature is reduced in amplitude slightly, and has a lower phase shift of about 1 h. The errors have magnitude of up to 0.09 °C.

Lastly, we look at the effects of moving to a 3-h coupling period, with timestep length maintained at 1 h (Fig. 3). It is apparent that this change has little effect on the phase or amplitude of the surface temperature simulation, and only serves to make the diurnal cycle more "jagged"; at each coupling period, indicated by the solid grey lines, the surface temperature jumps by a large amount, and over the following two (non-coupling) timesteps, moves backwards by a smaller amount as the sea ice adjusts towards a new equilibrium.

The error in the 4-layer experiment should give cause for concern, as this is a fairly realistic resolution for most implementations of CICE in coupled models. In the next

GMDD
8, 9707–9739, 2015

section, therefore, we compare the simulations at realistic resolution, using the two different coupling methods.

4 Comparing the two coupling methods under realistic resolution

4.1 Setup

For this experiment, the solver was run under 6 different setups. Firstly, two "control" experiments were undertaken, in which the ice, atmosphere and coupling timesteps were each 1 s. In the first control, the ice was given 100 layers, to provide a "truth" against which to compare subsequent experiments; in the second control, the ice was given 4 layers, to separate the effects of high timestep values from the effects of low vertical resolution. The two control experiments were run using the "CICE" coupling method, with the surface variables calculated by the ice model, but at these timestep values the coupling method has negligible impact on the simulation.

The solver was then run with 4 vertical layers, an ice timestep of 1 h, atmosphere timestep 20 min, and coupling period of 1 h, fairly realistic values for a coupled model, using the two different coupling methods, "CICE" and "JULES". A further two experiments were then performed, using a coupling period of 3 h, also a common period found in coupled model runs.

The solver was forced with incoming sensible heat flux only, driven by a diurnal cycle of atmospheric surface temperature $T_{\text{atmos}} = A_T \exp i\omega t$. For the "CICE" coupling, T_{atmos} is averaged over a coupling period and passed to the ice model, which calculates from this the incoming sensible heat flux, and uses this as forcing for the temperature solver to calculate internal and surface ice temperatures. For the "JULES" coupling, a self-contained "atmosphere model" uses T_{atmos} and T_1 (top-layer ice temperature) to implicitly calculate surface fluxes, including F_{condtop}, downwards conductive flux, accumulates and averages this over the coupling period and passes it to the ice model as forcing for the solver.

GMDD
8, 9707–9739, 2015

4.2 Results

4.2.1 1-h coupling

Figure 4 displays the simulation of key variables by the high-resolution control runs and by the test runs, using a 1-h coupling period length. The forcing atmospheric temperature is indicated in Fig. 4a. First examining the surface flux (Fig. 4b), we compare the two control runs and note that the decrease in vertical resolution is associated with a slight decrease in amplitude and a phase lag. We then see that when the "JULES" coupling method is used, there is little further error associated with the decrease in temporal resolution (blue line). When the "CICE" coupling method is used, however, there is an additional phase lag and amplitude decrease, and in addition the diurnal cycle becomes more jagged.

Interpreting these results, it is likely that the additional phase lag is a consequence of the atmosphere model "seeing" a surface flux calculated in the previous CICE coupling period, which is itself based on an atmospheric temperature valid for the period before that, up to 2 h previously. With the "JULES" method, however, the surface flux is able to respond immediately to the changing atmospheric temperature. There is a corresponding delay in the atmosphere model "sensing" the damping response of the top layer ice temperature to the changing surface flux. However, the resulting phase lead is tiny in comparison to the phase lag of the "CICE" method.

We now consider the atmosphere model surface temperature (Fig. 4c). In this variable, a decreasing vertical resolution is associated with an increase in amplitude and a phase lead. Again, using the "JULES" method, a decreasing temporal resolution makes little difference, causing a tiny phase lag and a slightly less smooth shape compared to the 4-layer control. Using the "CICE" method produces a much more blocky shape, and a substantial phase lag. However, as the 4-layer control itself has a phase lead relative to the high-resolution control, our "truth" the "CICE" method actually has a more accurate phase; the temporal and vertical errors "cancel", while the "JULES" method maintains a phase lead.

GMDD
8, 9707–9739, 2015

How the ice model "sees" the surface temperature is demonstrated in Fig. 4d. The diurnal cycle is very similar to that of the atmosphere model surface temperature for the two control runs, due to their low timestep length. The ice model does not have knowledge of the surface temperature in the "JULES" coupling method and this line is not plotted. The surface temperature simulation in the "CICE" method is very similar to the control; the phase lag experienced by the atmosphere model is due to the coupling delay only.

Conversely, Fig. 4e demonstrates how the atmosphere model "sees" the top layer temperature, in the 4-layer control and in the "JULES" coupling method (as in the "CICE" method the atmosphere has no knowledge of this variable). There is a slight phase lag relative to the control, and associated jaggedness of the diurnal cycle, owing to the need to hold the temperature constant over each coupling period, rather than update it every atmospheric timestep.

The lower panels (Fig. 4f and g) compare the internal ice temperatures at 0.125 m (top layer) and 0.625 m (third layer) depth in the four experiments. For both variables, the decrease in vertical resolution is characterised by a decrease in amplitude and a phase lead which are both more severe in the deeper variable. The decrease in timestep length produces additional amplitude decrease and phase lead which are very similar in the two coupling methods. It is interesting to note that the errors are marginally smaller for the "JULES" method. This is likely due to the fact that in the "JULES" method, changes in T_{atmos} can propagate quickly downwards to changes to f_{surf} on the 20 min atmospheric timestep, the main bottleneck occurring in the coupling, as f_{surf} forces changes in T_1 on the slower 1-h coupling period. In contrast, in the "CICE" method, each link in the chain – from T_{air}, to T_{sfc} and f_{condtop}, to T_1 – must communicate on a slow 1-h timestep. In consequence, the "JULES" method simulation is slightly closer to that of the 4-layer control.

GMDD
8, 9707–9739, 2015

4.2.2 3-h coupling

The results of the experiments when 3-h coupling is used are shown in Fig. 5. For the surface flux (Fig. 5b), again, decreasing temporal resolution is identified with a small phase lag and amplitude decrease in the "JULES" method; the simulation is very similar to that with the 1-h coupling period, although slightly less smooth. For the "CICE" method, however, the phase lag and amplitude decrease are greatly magnified; the peak of the diurnal cycle occurs 2–3 h too late, and the cycle has a very discontinuous shape.

Considering the surface temperature (Fig. 5c), the "JULES" method again produces a simulation with a 3-h coupling period which is quite similar to that with the 1-h period, though less smooth. Again the effect of the "CICE" method is to produce a phase lag. Whereas in the 1-h coupling period case, however, this phase lag almost exactly cancelled the lead of the increased vertical resolution, in the 3-h case the lead is much greater, and the absolute phase error of the method is actually greater than that of the "JULES" method, in an interesting demonstration of the dangers of cancelling errors.

When considering the ice variables (Fig. 5f and g) there are again few clear differences between the simulations, but again the error is marginally smaller for the "JULES" method than for the "CICE" method. Again this is likely related to the "chain" by which changes propagate from T_{atmos}, via T_{sfc} and f_{surf}, to T_1. The "JULES" method involves a "fast" link, on the 20 min atmospheric timestep, from T_{atmos} to T_{sfc} and f_{surf}, and a "very slow" link, on the 3-h coupling timestep, from f_{surf} to T_1. By contrast, the "CICE" method involves a "very slow" link, on the 3-h coupling timestep, from T_{atmos} to T_{sfc} and f_{surf}, and a "slow" link, on the 1-h CICE timestep, from T_{sfc} to T_1. While the rate of propagation is for both methods dominated by the 3-h coupling "bottleneck", therefore, changes in Tatmos are still able to propagate slightly more quickly with the "JULES" method. This is demonstrated schematically in Fig. 6.

In summary, the deterioration in simulation of the atmospheric variables that is associated with decreased temporal resolution is significantly reduced by using the "JULES"

GMDD
8, 9707–9739, 2015

coupling method. There is also a small improvement in the simulation of the ice variables, although this is very marginal.

5 Discussion and conclusions

This study has compared, under idealised conditions, the performance of the CICE temperature solver under varying resolutions, and using two different methods of coupling with an atmospheric model. It has been shown that low vertical resolution within the ice can be the source of significant errors in simulating the diurnal cycle. It has been shown that in simulating an idealised diurnal cycle of ice temperatures and surface fluxes, a coupled model in which an atmosphere–ice interface is placed within the ice performs considerably better than one in which an interface is placed at the ice surface, under typical temporal and vertical resolutions; the simulation of surface temperature and surface flux are in general significantly improved, and the simulation of within-ice variables also improves slightly.

This prompts the question: how realistic were the conditions under which the one-dimensional experiments were held, and to what degree would this improvement carry across to the simulation of ice and atmospheric variables in a non-idealised setting? Clearly the best way to answer this question would be to test two coupled models, one using each method. However, the differences between the two setups involve substantial structural changes to all components of the HadGEM3 model, and this option was deemed impractical. Following the results of these experiments, the "JULES" coupling method is being implemented in the Hadley Centre's coupled model HadGEM3 for use with CICE's capability for multilayer thermodynamics, and when this becomes operational there will be an opportunity to compare the simulation of processes over sea ice to other fully-coupled models which use CICE with the standard "CICE" coupling method. It is nevertheless possible to use the insight provided by the idealised experiments to gain some idea of the likely effects of the different coupling methods in a 3-D simulation.

GMDD
8, 9707–9739, 2015

The principal effect of the "CICE" coupling, as opposed to the "JULES" coupling, is to damp and delay the response of the surface flux (equal in these experiments to the sensitive heat flux) to changes in surface air temperature. These changes are applied in the experiments as variations of around 5 °C in the course of about 12 h. Variations in air temperature of this rate and magnitude are common in the Arctic Ocean, although often they occur in response to changes in cloud cover, or the passage of frontal boundaries, rather than to the diurnal cycle (e.g. Persson et al., 2002). Nevertheless, the implication of the 1-D experiments is that a model using the "CICE" coupling method will simulate a surface flux response that is overly delayed and damped, relative to a model using the "JULES" coupling. In effect, the coupling between the atmosphere and the underlying sea ice is weaker, and the atmosphere is likely to behave more like an isolated system.

The effects of this would be complex. A mild airmass moving over cold sea ice tends to be diabatically cooled at the surface via the surface flux response, while the opposite will occur when a cold airmass moves over less cold sea ice. A delayed and damped surface flux response would tend to reduce the rate of modification of airmasses, allowing them to retain characteristics for longer. A similar effect would be likely to be seen in the event of air temperatures responding to changes in radiative forcing due to cloud cover. Normally, the response of surface flux would likely be to moderate diabatic heating or cooling of air masses due to these radiative effects, by transferring some of this heating or cooling into the sea ice; a delayed, damped response would hinder this modification. In this way, it is possible that anomalous characteristics of neighbouring airmasses would become more exaggerated, relative to the real world, when using the "CICE" coupling method, with unpredictable consequences for atmospheric dynamics.

It is seen in Sect. 4 that the choice of coupling method has little direct impact on the internal sea ice simulation. However, the sea ice simulation will be strongly affected through the atmospheric response described above, whose dynamics will affect advection of warm and cold air over the ice, as well as advection of the ice itself. As the "JULES" coupling method produces a more realistic surface flux response to changes

GMDD
8, 9707–9739, 2015

in air temperature, it appears clear that, all other factors being equal, this coupling method would simulate a more accurate evolution of atmosphere and sea ice.

A secondary finding of this study has been that the vertical resolution at the top of the sea ice is of similar importance to the coupling method used in terms of simulating a realistic surface flux, as demonstrated in Fig. 4b. In the current configuration of CICE, whereby all layers are equally spaced within the ice, this implies that surface flux response will tend to be stronger, and more realistic, in regions of thin ice. This suggests that the implementation of variably-spaced layers, with higher resolution near the top of the ice, would be a logical objective to pursue subsequently, to further improve surface flux simulation.

The main focus of this study has been the accuracy of the two coupling methods; a separate question is their stability. The "CICE" method of coupling is known to have major problems of instability arising from the explicit interface in the surface exchange, an area where processes occur relatively quickly (e.g. Best et al., 2004). However, the "JULES" method has its own explicit interface, below the ice surface, and is therefore also likely to become unstable under certain conditions. A detailed analysis of the stability of the "JULES" method in the one-dimensional case is described in Appendix A. The principal factors affecting stability are found to be ice thickness and wind speed; a prediction from this analysis is that setting a minimum ice thickness of 30 cm in a coupled model is sufficient to avoid instability in all situations. In practice, however, in test runs of the coupled model a minimum ice thickness of 20 cm has been found to be sufficient to avoid instability. This is probably because in the fully-coupled model, other negative feedbacks are at work in the atmosphere that act to damp oscillations caused by the explicit coupling, and prevent instability.

It is planned to follow this paper with a study examining the simulation of sea ice in HadGEM3 resulting from the implementation of multilayer sea ice, using the "JULES" coupling method.

GMDD
8, 9707–9739, 2015

Appendix A: Stability of the "JULES" method of coupling

In this section, the one-dimensional model is used to investigate the conditions under which the solver becomes unstable, prior to its implementation in the Met Office coupled model.

In the stability experiment, the model was run for 5 days; for the first day, the atmospheric temperature was held constant at −20 °C, but at the beginning of the second day, the atmospheric temperature was abruptly changed to −15 °C; the solver was judged to be stable or unstable according to whether the variables converged to a new solution, and the nature of the convergence was examined. The test was performed under typical modelling conditions of 4 ice layers, ice timestep 1 h, atmospheric timestep 20 min, and of coupling period length 3 h. The initial parameter that was varied was the ice thickness; the test was performed for six different thicknesses of ice: 1 m, 20 cm, 10 cm, 5 cm, 1 cm and 1 mm. In each case, the top layer ice temperature converged to a new solution, the convergence tending to be most rapid for the thinnest ice (Fig. A1).

From this it appears that under normal modelling conditions, the "JULES" coupling method is not inherently unstable to sudden perturbations, and tends to be more, rather than less stable, for thin ice. This is perhaps surprising, as it would be thought that thin ice would tend to react more sensitively to perturbations in conductive flux, given its lower thermal inertia. However, counteracting this is the higher effective conductivity of thin ice, meaning that perturbations in top conductive flux will tend to propagate more rapidly through the ice during a coupling period, reducing the resulting change in top layer ice temperature. It also means that as ice thins, the response of the conductive flux comes to dominate the surface energy balance, effectively "locking" surface temperature to top layer ice temperature, and reducing variation in conductive flux.

To examine the reasons for the stability more carefully, we derive theoretical limits on perturbations to top layer temperature and conductive flux. Given an equilibrium solution to the coupled system $(F_{\mathrm{eq}}, T_{1\_\mathrm{eq}}, T_{\mathrm{sfc\_eq}})$, and perturbations around this solution $\left(\hat{F}, \hat{T}_1, \hat{T}_{\mathrm{sfc}}\right)$, it can be shown from the surface energy balance equation that the pertur-

GMDD
8, 9707–9739, 2015

bation conductive flux produced by the atmosphere is constrained by the perturbation top layer ice temperature in the following way:

$$|\hat{F}| \leq \frac{k_{\text{eff}}\text{OFE}}{k_{\text{eff}} + \text{OFE}} \cdot \left|\hat{T}_1\right| \tag{A1}$$

where $k_{\text{eff}} = \frac{2k_1}{h_1}$ is the effective conductivity of the top layer and $\text{OFE} = \dot{f}_{\text{sens}}(T_{\text{sfc\_eq}}) + \dot{f}_{\text{lat}}(T_{\text{sfc\_eq}}) + \dot{f}_{\text{rad}}(T_{\text{sfc\_eq}})$ represents the total rate of change of the surface radiative, sensible and latent heat fluxes with respect to surface temperature at $T_{\text{sfc}} = T_{\text{sfc\_eq}}$, and tends to reach its highest values under very windy, stormy conditions. It can be seen that the controlling constant here tends to the finite limit OFE as $h_1 \to 0$.

Meanwhile, in the ice thermodynamic solver, energy balance considerations provide a constraint on the magnitude of the change in $\hat{T}_1$ during a coupling period:

$$|\Delta T_1| \leq \frac{t_c}{c_p \rho_l h_1} |F| \tag{A2}$$

where t_c, c_p, ρ_l and h_1 represent coupling period length, ice heat capacity, ice density and top layer ice thickness respectively. This, together with Eq. (A1), prevents instability for $\frac{t_c \text{OFE}}{h_1} < c_p \rho_l$. The system is therefore stable for $h_1 > 5$ cm (equivalently total ice thickness < 20 cm) in all but the most extreme atmospheric conditions, and for $h_1 > 10$ cm (equivalently ice thickness < 40 cm) under all realistic atmospheric conditions.

However, for thin ice a second constraint becomes important. A dimensional analysis of the heat diffusion equation for ice shows that with 3-h coupling, the thermal inertia term can no longer provide the dominant balance to top conductive flux for ice of layer thickness under about 10 cm, and becomes negligible for ice of layer thickness under about 2 cm, causing the dominant balance in the equation to be between top conductive flux and conduction with the layer below. In this situation, given a top conductive forcing, the ice temperatures will converge very quickly to a linear temperature profile with

GMDD
8, 9707–9739, 2015

uniform conductive flux, meaning that

$$\left|\hat{T}_1\right| = \frac{h_1}{2k_1}\left|\hat{F}_1\right| \tag{A3}$$

Combined with Eq. (A1), this prevents instability completely.

In summary, Eqs. (A1)–(A3) show that instability cannot occur in the limit of very thick ice (when thermal inertia dominates), due to a highly damped response of top layer temperature to perturbations of conductive flux, and also cannot occur in the limit of very thin ice (when conduction to the ocean dominates), due to the surface temperature becoming virtually "locked" to top layer ice temperature, perturbations in conductive flux becoming correspondingly small (i.e. when $k_{\text{eff}} \gg$ OFE), and these perturbations very easily propagating through the ice to the ocean. It is noticeable that in Fig. A1, the least stable solutions appear to occur for intermediate ice thicknesses (5, 10 cm), when neither conduction nor thermal inertia dominates, but the "overlap" in the two conditions is nevertheless sufficient to allow a relatively rapid convergence.

The question arises as to whether the solver would continue to converge for all ice thicknesses were any of the parameters in Eqs. (A1), (A2) or (A3) altered. Parameters c_p, ρ_{I} and t_{c} are assumed to be at the lower, lower and upper limits of physical plausibility respectively in Eq. (2), and to vary them in the opposite direction would serve only to strengthen the limits on convergence. The parameter OFE, however, depends strongly on the rate of change of turbulent fluxes with respect to surface temperature, and therefore on wind speed. In the initial stability experiments, wind speed was set to $5\,\text{m}\,\text{s}^{-1}$, a fairly typical value for many synoptic situations. Particularly with the passage of extratropical depressions, however, wind speeds can reach much higher values.

The perturbation experiment was repeated, but this time two parameters were varied: ice thickness from 1 mm to 1 m, and wind speed from 0 to $50\,\text{m}\,\text{s}^{-1}$, the upper limit roughly representing the very highest wind speeds possible during extratropical storms. The results are shown in Fig. A2. It is seen that the solver is no longer unconditionally stable, with instability setting in at a wind speed of around $23\,\text{m}\,\text{s}^{-1}$, at first for a narrow

GMDD
8, 9707–9739, 2015

band of ice thicknesses close to 10 cm, a band which steadily widens as wind speed increases. At all wind speeds the solver remains stable in the limit of thin ice. However, at the upper limit of wind speed, the solver is unstable for ice thicknesses of between roughly 4 and 25 cm.

This result holds for t_c = 3 h, but t_c = 1 h is also a fairly widely used coupling period, and is likely to become more so as computing power increases. The experiment was repeated for t_c = 1 h (Fig. A3). In this case, the solver is stable for all ice thicknesses and wind speeds, although at the upper limit of wind speed, convergence is extremely slow for ice thicknesses of around 7 cm. (Clearly the second region of slow convergence, to the right of the figure, is not a concern, as this is caused by higher thermal inertia of thick ice, is entirely physically realistic, and will not lead to instability).

In summary, it is found that the coupled solver system is stable under all physically realistic situations when 1-h coupling is used, but may become unstable in very windy conditions when 3-h coupling is used, for certain values of ice thickness.

Author contributions. The "JULES" method of coupling was originally devised by Martin Best. The one-dimensional experiments of Sects. 3 and 4 were designed and carried out by Alison McLaren. The stability experiments of the Appendix were designed and carried out by Alex West. All results were plotted and analysed by Alex West with advice and assistance from Alison McLaren, Martin Best and Helene Hewitt. The paper was written in its final form by Alex West with input from all three contributing authors.

Acknowledgements. Thanks to Ann Keen and Ed Blockley for help and advice prior to submission.

This study was supported by the Joint UK DECC/Defra Met Office Hadley Centre Climate Programme (GA01101).

References

Best, M. J., Beljaars, A., Polcher, J., and Viterbo, P.: A proposed structure for coupling tiled surfaces with the planetary boundary layer, J. Hydrometeorol., 5, 1271–1278, doi:10.1175/JHM-382.1, 2004.

GMDD

8, 9707–9739, 2015

Best, M. J., Cox, P. M., and Warrilow, D. M.: Determining the optimal soil temperature scheme for atmospheric modelling applications, Bound.-Lay. Meteorol., 114, 111–142, 2005.

Best, M. J., Pryor, M., Clark, D. B., Rooney, G. G., Essery, R. L. H., Ménard, C. B., Edwards, J. M., Hendry, M. A., Porson, A., Gedney, N., Mercado, L. M., Sitch, S., Blyth, E., Boucher, O., Cox, P. M., Grimmond, C. S. B., and Harding, R. J.: The Joint UK Land Environment Simulator (JULES), model description – Part 1: Energy and water fluxes, Geosci. Model Dev., 4, 677–699, doi:10.5194/gmd-4-677-2011, 2011.

Bitz, C. M. and Lipscomb, W. H.: An energy-conserving thermodynamic model of sea ice, J. Geophys. Res., 104, 15669–15677, 1999.

Gordon, C., Cooper, C., Senior, C. A., Banks, H., Gregory, J. M., Johns, T. C., Mitchell, J. F. B., and Wood, R. A.: The simulation of SST, sea ice extents and ocean heat transports in a version of the Hadley Centre coupled model without flux adjustments, Clim. Dynam., 16, 147–168, doi:10.1007/s003820050010, 2000.

Hewitt, H. T., Copsey, D., Culverwell, I. D., Harris, C. M., Hill, R. S. R., Keen, A. B., McLaren, A. J., and Hunke, E. C.: Design and implementation of the infrastructure of HadGEM3: the next-generation Met Office climate modelling system, Geosci. Model Dev., 4, 223–253, doi:10.5194/gmd-4-223-2011, 2011.

Hunke, E. C., Lipscomb, W. H., Turner, A. K., Jeffery, N., and Elliott, S.: CICE: the Los Alamos Sea Ice Model, Documentation and Software, Version 5.0, Los Alamos National Laboratory Tech. Rep. LA-CC-06-012, Los Alamos, New Mexico, available at: http://oceans11.lanl.gov/trac/CICE/attachment/wiki/WikiStart/cicedoc.pdf?format=raw (last access: 27 October 2015), 2013.

Johns, T. C., Durman, C. F., Banks, H. T., Roberts, M. J., McLaren, A. J., Ridley, J. K., Senior, C. A., Williams, K. D., Jones, A., Rickard, G. J., C. S., Ingram, W. J., Crucifix, M., Sexton, D. M. H., Joshi, M. M., Dong, B.-W., Spencer, H., Hill, R. S. R., Gregory, J. M., Keen, A. B., Pardaens, A. K., Lowe, J. A., Bodas-Salcedo, A., Stark, S., and Searl, Y.: The New Hadley Centre Climate Model (HadGEM1): evaluation of coupled simulations, J. Climate, 19, 1327–1353, doi:10.1175/JCLI3712.1, 2006.

Maykut, G. A. and Untersteiner, N.: Some results from a time-dependent thermo-dynamic model of sea ice, J. Geophys. Res., 7, 1550–1575, 1971.

Ono, N.: Specific heat and fusion of sea ice, in: Physics of Snow and Ice, 1, 599–610, 1967.

GMDD
8, 9707–9739, 2015

Persson, P. O. G., Fairall, C. W., Andreas, E. L., Guest, P. S., and Perovich, D. K.: Measurements near the Atmospheric Surface Flux Group tower at SHEBA: near-surface conditions and surface energy budget, J. Geophys. Res., 107, 8045, doi:10.1029/2000JC000705, 2002.

Semtner, A. J.: A model for the thermodynamic growth of sea ice in numerical investigations of climate, J. Phys. Oceanogr., 6, 379–389, 1975.

Untersteiner, N.: Calculations of temperature regime and heat budget of sea ice in the Central Arctic, J. Geophys. Res., 69, 4755–4766, 1964.

Walters, D. N., Best, M. J., Bushell, A. C., Copsey, D., Edwards, J. M., Falloon, P. D., Harris, C. M., Lock, A. P., Manners, J. C., Morcrette, C. J., Roberts, M. J., Stratton, R. A., Webster, S., Wilkinson, J. M., Willett, M. R., Boutle, I. A., Earnshaw, P. D., Hill, P. G., MacLachlan, C., Martin, G. M., Moufouma-Okia, W., Palmer, M. D., Petch, J. C., Rooney, G. G., Scaife, A. A., and Williams, K. D.: The Met Office Unified Model Global Atmosphere 3.0/3.1 and JULES Global Land 3.0/3.1 configurations, Geosci. Model Dev., 4, 919–941, doi:10.5194/gmd-4-919-2011, 2011.

GMDD
8, 9707–9739, 2015

Table 1. Initial experiments comparing CICE under 6 different resolutions.

Experiment	Vertical resolution	Timestep length	Coupling period length
1 (Hi-res 1S)	1 cm (100 layers)	1 s	1 s
2 (Low-res 1S)	25 cm (4 layers)	1 s	1 s
3 (Hi-res 1H)	1 cm (100 layers)	1 h	1 h
4 (Low-res 1H)	25 cm (4 layers)	1 h	1 h
5 (Hi-res 3H)	1 cm (100 layers)	1 h	3 h
6 (Low-res 3H)	25 cm (4 layers)	1 h	3 h

GMDD
8, 9707–9739, 2015

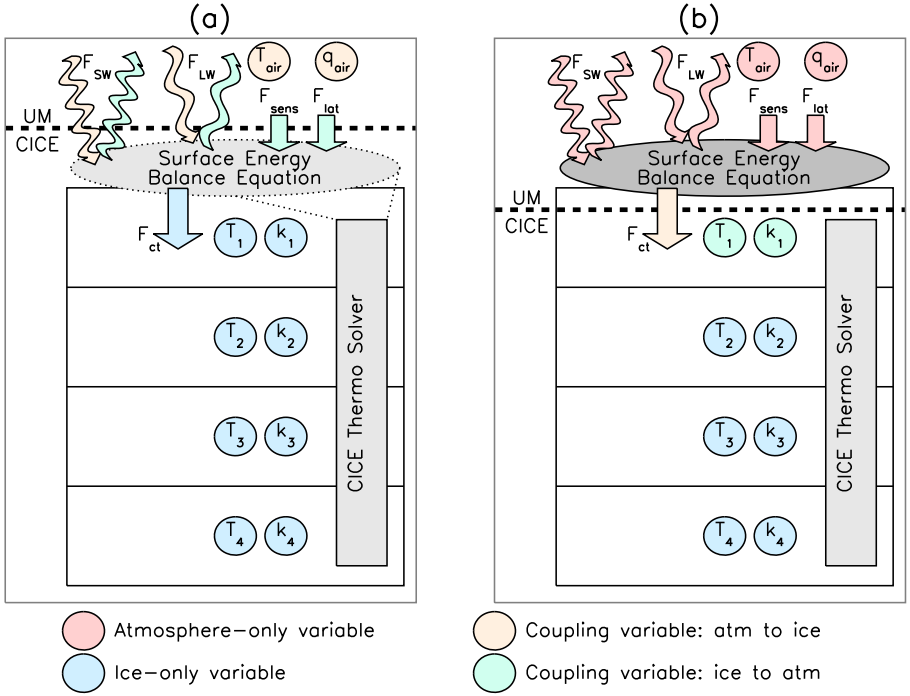

Figure 1. Schematics demonstrating **(a)** The "CICE" coupling method; **(b)** the "JULES" coupling method. In this figure F_{SW}, F_{LW}, F_{sens} and F_{lat} denote fluxes of shortwave radiation, longwave radiation, sensible and latent heat respectively, F_{ct} the conductive flux from the surface to the ice, T_{air} and q_{air} the temperature and humidity of the lowest atmospheric layer, and T_j and k_j, the temperature and effective conductivity of ice layer j.

GMDD
8, 9707–9739, 2015

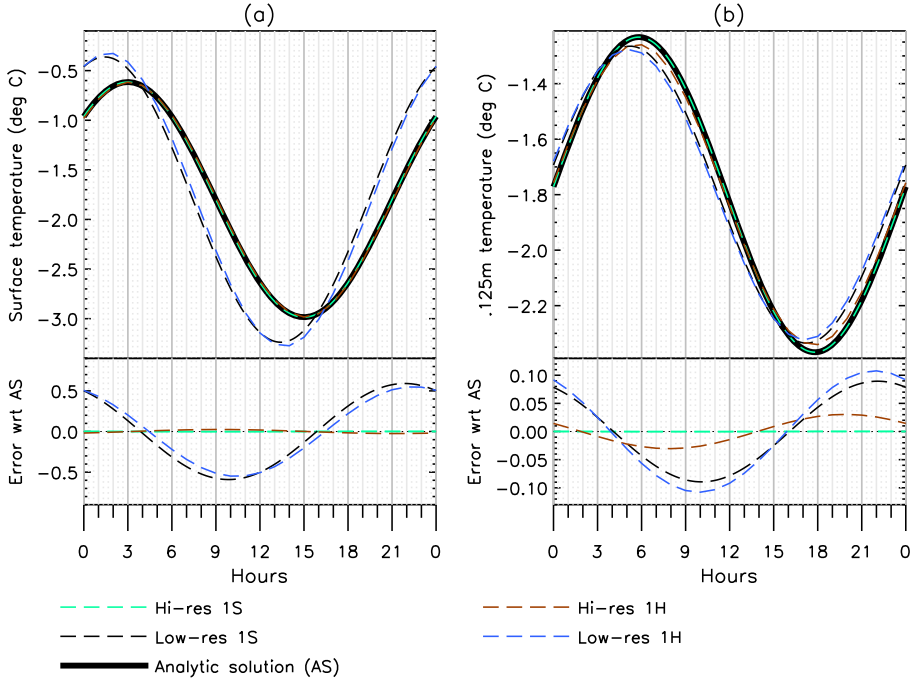

Figure 2. The performance of the CICE temperature solver under varying spatial resolution and timestep length, with coupling period 1 h. Showing **(a)** surface temperature; **(b)** temperature at 0.125 m depth.

GMDD
8, 9707–9739, 2015

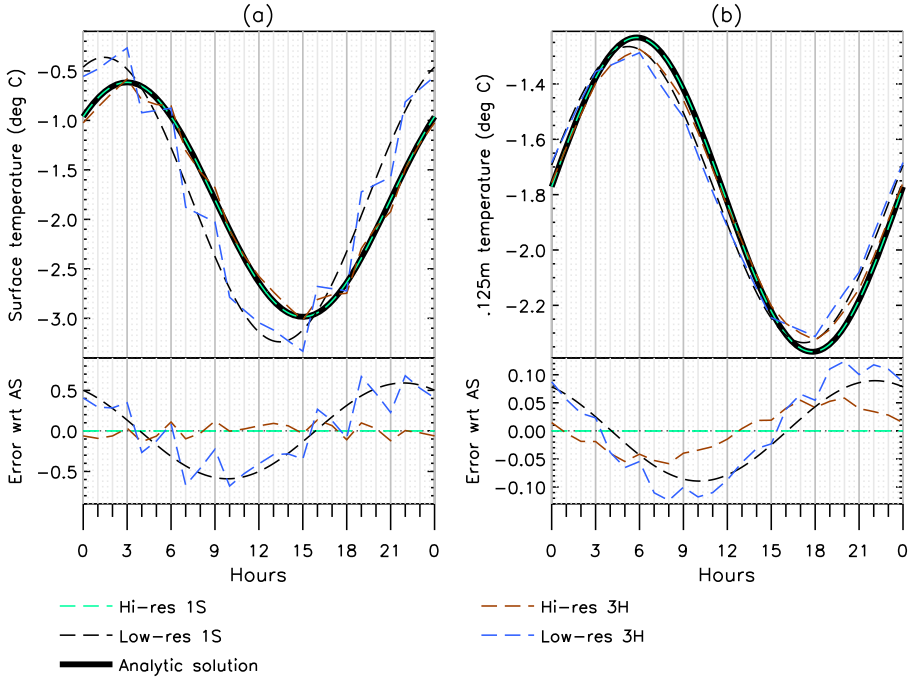

Figure 3. The performance of the CICE temperature solver under varying spatial resolution and timestep length, with coupling period 3 h. Showing **(a)** surface temperature; **(b)** temperature at 0.125 m depth.

GMDD
8, 9707–9739, 2015

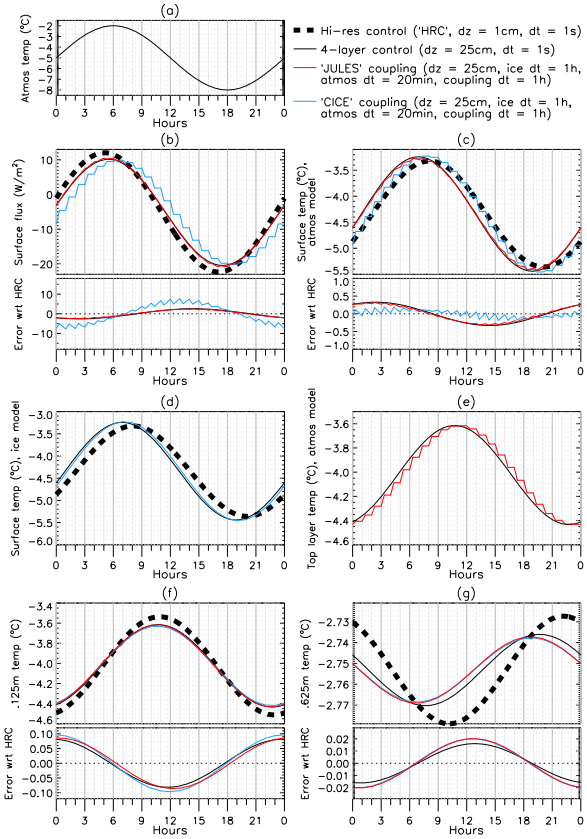

Figure 4. Comparing the two coupling methods, with a 1-h coupling period. Showing **(a)** atmospheric air temperature (the experiment forcing); **(b)** surface flux; **(c)** surface temperature, as seen by the atmosphere; **(d)** surface temperature as seen by the ice; **(e)** 0.125 m ice temperature as seen by the atmosphere; **(f)** 0.125 m temperature as seen by the ice; **(g)** 0.625 m temperature.

GMDD
8, 9707–9739, 2015

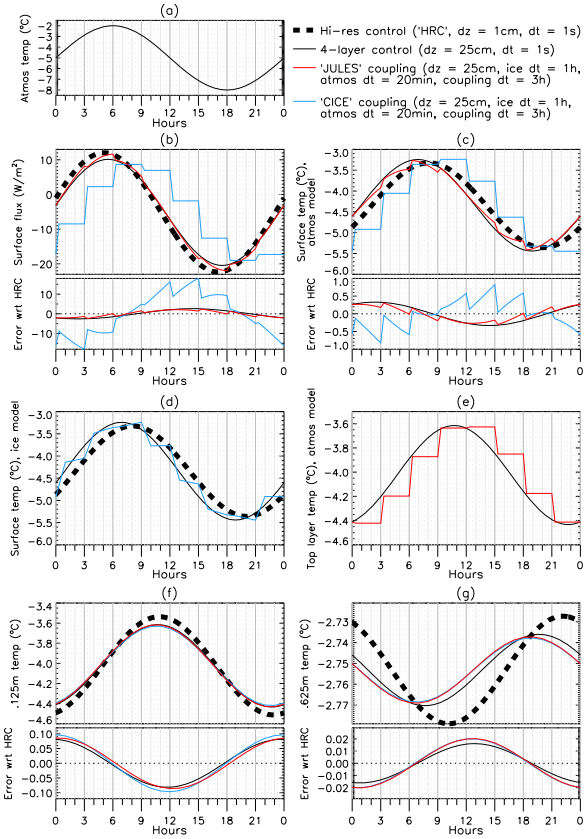

Figure 5. Comparing the two coupling methods, with a 3-h coupling period. Showing **(a)** atmospheric air temperature (the experiment forcing); **(b)** surface flux; **(c)** surface temperature, as seen by the atmosphere; **(d)** surface temperature as seen by the ice; **(e)** 0.125 m ice temperature as seen by the atmosphere; **(f)** 0.125 m temperature as seen by the ice; **(g)** 0.625 m temperature.

GMDD
8, 9707–9739, 2015

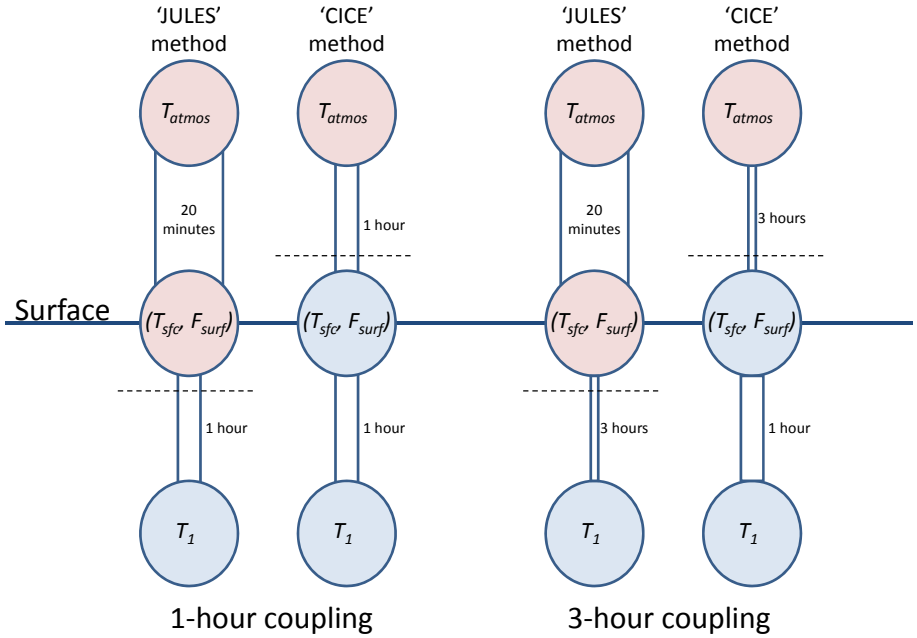

Figure 6. Demonstrating how quickly information regarding changes in variables can propagate downwards through the atmosphere–ice interface in the two coupling methods. The width of each "pipe" is inversely proportional to the timestep length in each case.

GMDD
8, 9707–9739, 2015

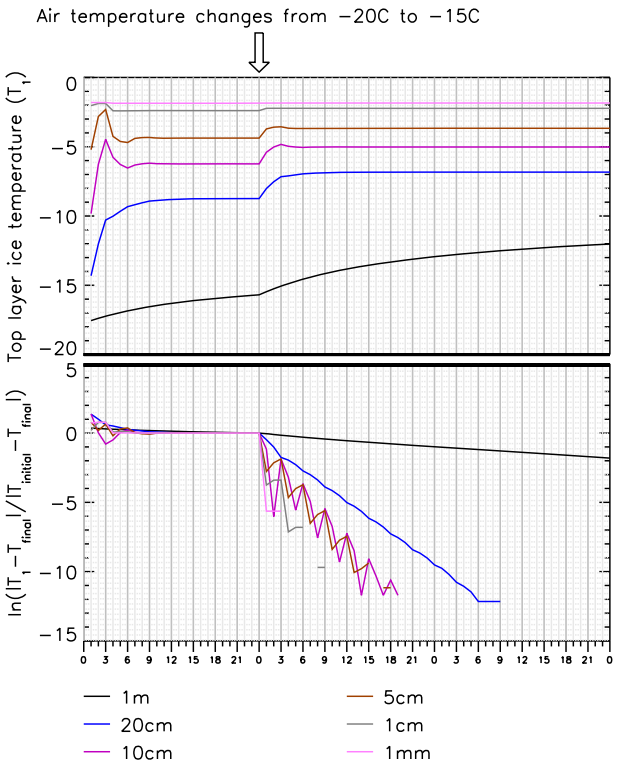

Figure A1. Showing the evolution of top layer ice temperature following a sudden change in air temperature, under the "JULES" coupling method. The lower panel shows the evolution of $\ln\left(\frac{|T_1 - T_{final}|}{|T_{initial} - T_{final}|}\right)$ to allow easy comparison of the rates of convergence for differing ice thicknesses, where T_1, T_{final} and $T_{initial}$ respectively refer to the evolving top layer ice temperature, the value of top layer ice temperature after 3 days, and the value at 1 day, at the time of the perturbation. The graph "disappears" when the difference falls below minimum precision.

GMDD
8, 9707–9739, 2015

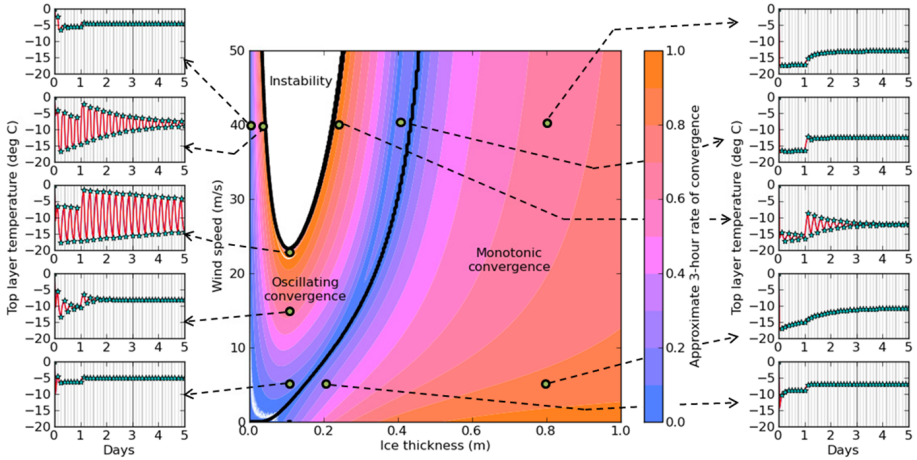

Figure A2. "Map" of stability of the coupled ice and surface solvers, as ice thickness and wind speed are varied, with a 3-h coupling period. Speed of convergence is indicated in colour, with blue = rapid convergence, red = slow convergence. Regions of 3-h monotonic convergence, 3-h oscillating convergence and instability are indicated. Timeseries of top layer ice temperature are shown for 10 representative points of the variable space.

GMDD
8, 9707–9739, 2015

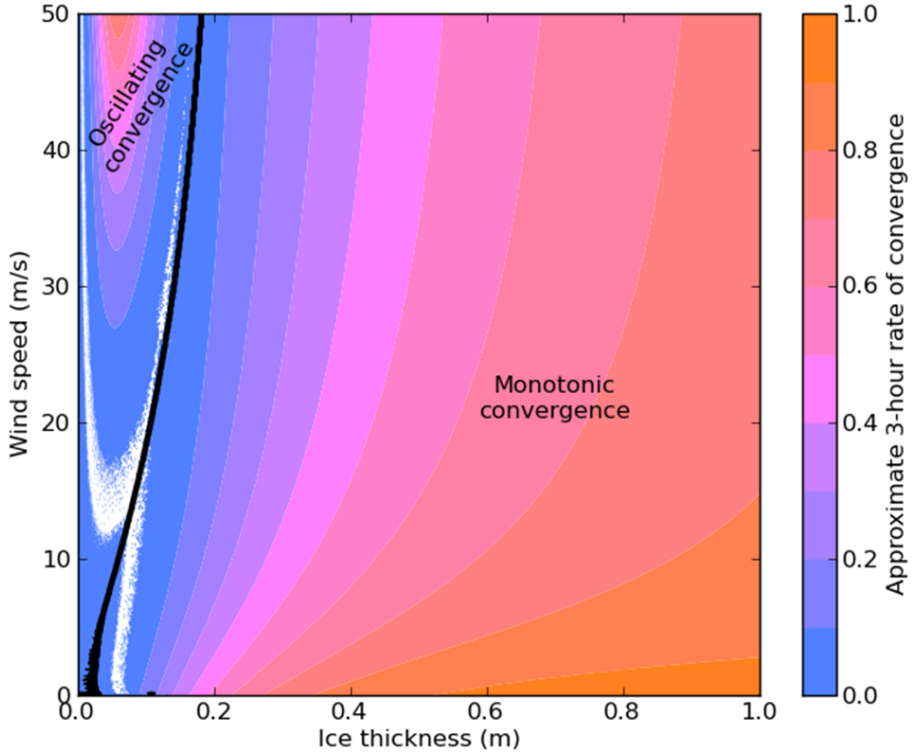

Figure A3. "Map" of stability of the coupled ice and surface solvers, as ice thickness and wind speed are varied, with a 1-h coupling period.

GMDD
8, 9707–9739, 2015